

PHYSICAL REVIEW A

ATOMIC, MOLECULAR, AND OPTICAL PHYSICS

THIRD SERIES, VOLUME 47, NUMBER 5 PART B

MAY 1993

ARTICLES

Xe L and M x-ray emission following Xe^{44–48+} ion impact on Cu surfaces

M. W. Clark,* D. Schneider, D. Dewitt, and J. W. McDonald

Lawrence Livermore National Laboratory, University of California, Livermore, California 94550

R. Bruch

University of Nevada, Reno, Reno, Nevada 89557

U. I. Safronova and I. Yu. Tolstikhina

Institute of Spectroscopy, Russian Academy of Sciences, Troitsk, 142092, Moscow Region, Russia

R. Schuch

Manne Siegbahn Institute of Physics, S-10405 Stockholm, Sweden

(Received 24 April 1992)

The x-ray emission following the impact of highly charged Xe ^{q +} ($q = 44–48$) ions of 7-keV/ q energy on a Cu surface has been measured. Theoretically we have derived an analytic formula which allows us to calculate the $2l-nl'$, $3l-nl'$, and $4l-nl'$ ($n \leq 5$), L , M , and N x-ray transition energies averaged over spin and angular-momentum quantum numbers (L and S) as a function of the electron occupation numbers (k_i) for the states $Q = 1s^{k_1}2s^{k_2}2p^{k_3}3s^{k_4}3p^{k_5}3d^{k_6}4s^{k_7}4p^{k_8}4d^{k_9}4f^{k_{10}}5s^{k_{11}}5p^{k_{12}}$. In accordance with our theoretical predictions the observed L x-ray structures shift toward higher energies and increase in intensity relative to the M x rays with increasing charge state. We have also observed an increase in high-energy satellite-line intensities with the increasing number of $2p$ vacancies. In calculating the radiative-transition probabilities we have found that the dominating electric-dipole transitions for L and M x rays are of the kind $2p-3d$ and $3d-4f$, respectively. A comparison between measured peak positions and calculated transition energies reveals that direct feeding by approximately 13 electrons can explain the main features of the observed x-ray emission spectra.

PACS number(s): 31.50.+w, 32.30.Rj, 79.20.Rf

I. INTRODUCTION

Much effort is presently directed towards research on ion-surface interactions using very highly charged ions [1]. This research became feasible with the development of new and advanced ion sources such as electron cyclotron resonance (ECR) sources, the electron-beam ion source (EBIS), and the electron-beam ion trap (EBIT) [2–6]. The EBIT is essentially very similar to an EBIS, except for the difference in the length of the electron-ion interaction path. Both ion sources use the principle of producing highly charged ions via successive ionization of atoms with intense energetic electron beams. The recently developed technique [2] to extract highly charged ions from the EBIT, which has been originally designed

as an ion trap, allows the use of ions up to Th⁸⁰⁺ for ion-surface interaction studies. These studies are mainly aimed at understanding the neutralization dynamics of highly charged ions as they approach the surface and penetrate into the solid. Such highly charged projectile ions carry up to several hundred keV potential energy and x-ray emission studies are particularly suited to illuminate the different interaction processes which lead to the transfer of this energy to the surface. Furthermore, such new experiments allow the observation of surface modifications induced by a medium-to-heavy ion impact. A more complete picture may eventually emerge from the simultaneous measurements of the Auger-electron and x-ray emission, sputter-ion yields, and the charge exchange of the projectile ion following the ion-surface in-

teraction [3–16]. X-ray emission has been measured with low resolution for $\text{Ne}^{9+,10+}$, $\text{Ar}^{17+,18+}$, and Kr^{36+} ion impact on surfaces. For the cases of Ne^{9+} and $\text{Ar}^{17+,18+}$ ions, high-resolution measurements using crystal spectrometers have been conducted. From these measurements the occurrence of “hollow atoms” during the neutralization process has been inferred [3]. Such superexcited states with nearly empty core levels are created mainly at small ion approach velocities where the ion-surface interaction is dominant. Multiple inner-shell vacancy states provide time windows to study stepwise deexcitation and the transfer of excitation energy to the reaction products. In particular, the satellite intensities and energy positions of the emitted x rays and Auger electrons provide important information on the history of the projectile ions interacting with the surface and the bulk material. In these types of studies the following physical processes and parameters are of major importance.

(a) The initial electronic configuration of the approaching ion and the surface potential of the solid determine the transfer of electrons from the surface into states with high- n quantum numbers.

(b) The approach velocity and the autoionization and radiative-decay rates determine the transfer of electrons to lower states or back to the solid, and together with (a) determine the distribution and time evolution of the population of different quantum states during neutralization.

(c) Transfer of electrons into a state with low quantum numbers occurs when the ion enters the surface.

A method to vary the ion-velocity component normal to surface, which has been used for $\text{Ne}^{9+,10+}$ and $\text{Ar}^{17+,18+}$ ion impact, is based on the change of the angle of ion impact between normal and grazing incidence. From an analysis of the corresponding K x-ray emission spectra (energy shifts and satellite-line intensities) the remaining number of inner-shell vacancies can be extracted. These results are generally very similar to those where the ions have been decelerated first to low velocity and then hit the surface at normal incidence. The ion-bulk interaction is more pronounced at higher approach velocities. In this case the inner-shell vacancies have a larger probability to penetrate the first surface layer and the interaction with the bulk may cause a fast filling of shells with lower- n quantum numbers with a simultaneous “peeling off” of electrons in shells with higher- n manifolds. States with intermediate- n quantum numbers can be filled either directly by electron transfer from the solid or by radiative or autoionizing decays. The balance between electron transfer and loss rates, autoionization and radiative transition rates, the approach velocity and the binding energies of the target and the projectile determine the specific population of n manifolds and the observed spectral-line intensities. We note that the innermost atomic shells are generally not filled by electron-capture reactions if the projectile velocity is too slow for direct electron transfer to occur. In this case surviving multiple inner-shell vacancy states can be used as an “inner atomic clock.” This idea has been first applied by Briand *et al.* [3] studying satellite and hypersatellite K x-ray transitions in bare Ar ion-surface collisions.

In this paper we present data on the ion-surface neutralization dynamics using more highly charged Xe ions, characterized by an approach velocity of $v \approx 0.22$ a.u. corresponding to $7 \text{ \AA}/\text{fs}$, where the number of L -shell vacancies in the incident Xe^{q+} ($q=44$ to 48) projectile is systematically changed. Here, $q=44+$ represents the closed shell $1s^2 2s^2 2p^6$ ground-state configuration of Xe and the other charge states are characterized by open L -shell configurations of the type $1s^2 2s^2 2p^5$ ($q=45+$), $1s^2 2s^2 2p^4$ ($q=46+$), $1s^2 2s^2 2p^3$ ($q=47+$), and $1s^2 2s^2 2p^2$ ($q=48+$) differing in the incident number of $2p$ holes.

As a first attempt to study experimentally the decay of highly excited Xe ions in the vicinity of a Cu surface, we have measured the L and M x-ray spectra as a function of the incident charge state. The experimental procedure is described in Sec. II. The description of the theoretical method used to predict radiative-transition energies and transition probabilities for Xe ions with different numbers of L -shell vacancies is presented in Sec. III. A more detailed description of our theoretical approach is given elsewhere [17]. A comparison of the predicted theoretical data with experimental results is presented in Sec. IV. Finally, the general trends of the experimental findings and important conclusions on the ion-surface and ion-bulk neutralization dynamics for the Xe^{q+} -plus-Cu system are discussed in Sec. V.

II. EXPERIMENT

In this paper we report measurements on ion-surface interactions for the impact of highly charged ions Xe^{q+} ($q=44$ – 48) on a solid surface. The Xe^{q+} ions have been extracted from the Lawrence Livermore EBIT source. In this work we only briefly address the operation of an EBIT and its upgrade to an ion source by means of an efficient extraction system which is described in detail in Ref. [2]. The EBIT basically consists of a three-segment axial drift-tube assembly. These segments may be individually biased to create an electrostatic well along the central axis. An electron beam, compressed to $\approx 70 \mu\text{m}$ in a 3-T magnetic field, travels along the central axis. The energy of the electrons is determined by the voltage applied to the drift-tube assembly. Typical electron-beam currents used range from 5 to 160 mA. Neutral gas atoms, such as Xe, are highly ionized by multiple electron impact and then trapped axially within the central well of the drift-tube potential and radially by the electron-beam space charge. After some confinement time they reach an equilibrium charge-state distribution due to successive ionization, excitation, recombination, and other ion-atom, ion-ion, and ion-electron interactions. After equilibrium is reached ($\tau \lesssim 1$ sec) the ions are ejected from the trap by applying an ejection voltage (e.g., 7 kV) to the drift-tube potentials and by raising the middle drift-tube potential. The ejected ions with energies given by the extraction voltage times the charge state q are then momentum analyzed and focused onto the target surface. In the present case the target surface was Cu which has been polished ($\approx 10 \mu\text{m}$ roughness) but not chemically or sputter cleaned. The target is tilted by 45° with respect to the ion-beam axis and the x-ray emission

following electron capture and loss of the ions at the surface is observed with a Si(Li) detector perpendicular to the beam axis. The geometrical solid angle of this detector was 3×10^{-3} sr and its resolution about 170 eV at 5.9 keV, respectively. The detector was separated from the target chamber vacuum by Be foils (total thickness: 0.075 mm). For the Xe *L* x-ray line structures around 4.5 keV, photon absorption in the Be window is negligible. However, for the Xe *M* radiation at around 2 keV the observed line intensities are reduced by a factor of approximately 2 due to absorption.

The vacuum in the beam-transport system between the EBIT and the analyzing magnet was about 10^{-8} Torr and the charge change by electron capture from rest gas molecules was estimated to be small. Between the magnet and the Cu target a vacuum of the order of 10^{-8} Torr was maintained leading to an estimated loss of ions with inner-shell vacancies of less than 10%.

III. ENERGIES OF A MANY-ELECTRON SYSTEM

The calculation of theoretical x-ray spectra, including transition probabilities and autoionization rates for multiply excited Xe ions with up to 53 electrons represents a challenging many-body problem [17–29]. In this work we have performed comprehensive calculations of transition energies and transition probabilities associated with multiply excited states in Xe by using nonrelativistic and relativistic perturbation theory [24–28].

In particular, we have studied electric-dipole transitions of the type $2l-3l'$, $2l-4l'$, $2l-5l'$, $3l-4l'$, $3l-5l'$, and $4l-5l'$ for configurations

$$Q = 1s_1^k 2s_2^k 2p_3^k 3s_4^k 3p_5^k 3d_6^k 4s_7^k 4p_8^k 4d_9^k 4f_{10}^k 5s_{11}^k 5p_{12}^k, \quad (1)$$

with up to $N=53$ electrons occupying 12 different subshells, where k_i ($i=1$ to 12) are the electron occupation numbers. Our method allows the expression of the desired atomic properties in analytical form as a function

of the electron numbers (k_i). As an important example we focus in this paper on x-ray energies and transition probabilities. The procedure to derive the nonrelativistic part of x-ray energies is outlined in the following.

A. Nonrelativistic part

In order to reduce the vast number of possible states, we have averaged over the spin and angular-momentum quantum numbers. These *LS*-averaged energy values can be expressed in first-order perturbation theory as [26]

$$E_1^N(Q) = \frac{1}{2} \sum_i k_i (k_i - 1) U(n_i l_i) + \sum_{i,j} k_i k_j U(n_i l_i, n_j l_j), \quad (2)$$

where the two-particle energies $U(nl), U(nl, n'l')$ are equal to

$$U(nl) = F_0(nl) \sum_{k(>0)} \frac{2l+1}{4l+1} \begin{bmatrix} l & l & k \\ 0 & 0 & 0 \end{bmatrix}^2 F_k(nl, nl), \quad (3)$$

$$U(nl, n'l') = F_0(nl, n'l') - \frac{1}{2} \sum_k \begin{bmatrix} l & l' & k \\ 0 & 0 & 0 \end{bmatrix}^2 G_k(nl, n'l'), \quad (4)$$

and the radial integrals are determined in the usual way [24]

$$F_k(nl, n'l') = R_k(nln'l'; n'l'nl),$$

$$G_k(nl, n'l') = R_k(nln'l'; nln'l'),$$

$$R_k(n_1 l_1 n_2 l_2; n_4 l_4 n_3 l_3)$$

$$= \int_0^\infty r_1^2 dr_1 \int_0^\infty r_2^2 dr_2 \frac{r_1^k}{r_2^{k+1}} R_{n_2 l_2}(r_2)$$

$$\times R_{n_4 l_4}(r_2) R_{n_3 l_3}(r_1) R_{n_1 l_1}(r_1). \quad (5)$$

Substituting into (2) the numerical values for the radial integrals, we obtain for $E_1(Q)$

$$\begin{aligned} E_1^N(Q) = & \frac{k_1}{2} (k_1 - 1) 0.625 + \frac{k_2}{2} (k_2 - 1) 0.150391 + \frac{k_3}{2} (k_3 - 1) 0.174609 + \frac{k_4}{2} (k_4 - 1) 0.0664062 \\ & + \frac{k_5}{2} (k_5 - 1) 0.0689888 + \frac{k_6}{2} (k_6 - 1) 0.0836637 + \frac{k_7}{2} (k_7 - 1) 0.0372715 \\ & + \frac{k_8}{2} (k_8 - 1) 0.0373409 + \frac{k_9}{2} (k_9 - 1) 0.0412849 + \frac{k_{10}}{2} (k_{10} - 1) 0.0491365 \\ & + \frac{k_{11}}{2} (k_{11} - 1) 0.0238300 + \frac{k_{12}}{2} (k_{12} - 1) 0.0228084 + k_1 k_2 0.198904 + k_1 k_3 0.234263 \\ & + k_1 k_4 0.0966034 + k_1 k_5 0.106560 + k_1 k_6 0.110899 + k_1 k_7 0.0564634 + k_1 k_8 0.0605942 \\ & + k_1 k_9 0.0623842 + k_1 k_{10} 0.0624983 + k_1 k_{11} 0.036928 + k_1 k_{12} 0.0390275 \\ & + k_2 k_3 0.147461 + k_2 k_4 0.0803759 + k_2 k_5 0.0885966 + k_2 k_6 0.0999259 \\ & + k_2 k_7 0.0501547 + k_2 k_8 0.0535040 + k_2 k_9 0.0580181 + k_2 k_{10} 0.0618372 + k_2 k_{11} 0.033794 \\ & + k_2 k_{12} 0.0354930 + k_3 k_4 0.0851854 + k_3 k_5 0.0915985 + k_3 k_6 0.102905 + k_3 k_7 0.0518611 \\ & + k_3 k_8 0.0547236 + k_3 k_9 0.0591497 + k_3 k_{10} 0.0621009 + k_3 k_{11} 0.0346135 + k_3 k_{12} 0.03611 \\ & + k_4 k_5 0.0617407 + k_4 k_6 0.0708551 + k_4 k_7 0.0430152 + k_4 k_8 0.045800 + k_4 k_9 0.049052 \end{aligned}$$

$$\begin{aligned}
&+k_4k_{10}0.0544346+k_4k_{11}0.0305275+k_4k_{12}0.0318306+k_5k_60.073622+k_5k_70.0448665 \\
&+k_5k_80.0464013+k_5k_90.0502083+k_5k_{10}0.0555011+k_5k_{11}0.0312566+k_5k_{12}0.0321604 \\
&+k_6k_70.0467491+k_6k_80.048611+k_6k_90.0523995+k_6k_{10}0.0585227+k_6k_{11}0.0321045 \\
&+k_6k_{12}0.0331316+k_7k_80.0298844+k_7k_90.0379267+k_7k_{10}0.040885+k_7k_{11}0.026676 \\
&+k_7k_{12}0.0279655+k_8k_90.0384131+k_8k_{10}0.04151+k_8k_{11}0.0276224+k_8k_{12}0.0281404 \\
&+k_9k_{10}0.0441092+k_9k_{11}0.0284508+k_9k_{12}0.0290856+k_{10}k_{11}0.0294274 \\
&+k_{10}k_{12}0.0301394+k_{11}k_{12}0.0215045.
\end{aligned} \tag{6}$$

In zero approximation a simple expression has been derived for the energy of each Q state,

$$E_0^N(Q) = -\frac{1}{2} \left[k_1 + \frac{k_2+k_3}{4} + \frac{k_4+k_5+k_6}{9} + \frac{k_7+k_8+k_9+k_{10}}{16} + \frac{k_{11}+k_{12}}{25} \right]. \tag{7}$$

$E_0^N(Q)$ and $E_1^N(Q)$ are generally not very good approximations for any atomic system; however, the accuracy of the method can be improved by using the following screening approach:

$$E^N(Q) = E_0^N(Q) \left[Z + \frac{E_1^N(Q)}{2E_0^N(Q)} \right]^2, \tag{8}$$

which incorporates part of the second-order approximation.

It was shown [27] that almost 90% of E_2^N was actually taken into account by using the above formula. The same type of screening procedure can be applied for the calculation of $n_1l_1-n_2l_2$ x-ray transition energies, namely,

$$\begin{aligned}
&E^N(Q) - E^N([n_1l_1]^{-1}n_2l_2Q) \\
&\cong Z^2[E_0^N(n_1l_1) - E_0^N(n_2l_2)] \\
&\quad + Z\{E_1^N(Q) - E_1^N([n_1l_1]^{-1}n_2l_2Q)\} \\
&= [E_0^N(n_1l_1) - E_0^N(n_2l_2)](Z - \sigma^N)^2, \\
&\quad - \{E_1^N(Q) - E_1^N([n_1l_1]^{-1}n_2l_2Q)\}, \\
\sigma^N &= \frac{2[E_0^N(n_1l_1) - E_0^N(n_2l_2)]}{2[E_0^N(n_1l_1) - E_0^N(n_2l_2)]}, \tag{9}
\end{aligned}$$

$$E^N(nl) = -1/2n^2.$$

In the calculations performed in this work, n_1l_1, n_2l_2 are fixed and the occupation numbers k_i of electrons in each subshell varied. Specifically, we have adopted the following notation for each initial inner-hole state, namely:

$$[n_1l_1]^{-1}n_2l_2Q, \tag{10}$$

where $[n_1l_1]^{-1}$ characterizes the inner-shell vacancy to be filled, n_2l_2 the active electron involved in the electric-dipole transition, and Q represents the additional spectator electrons distributed over various subshells.

B. Relativistic corrections

For intermediate- Z atoms, like Xe, relativistic effects may be accounted for by adding additional terms to the

nonrelativistic Hamiltonian resulting from the reduction of the Dirac equation and the Breit interaction [29]. Since we are interested in LS -averaged energies, only those terms of the Breit operator which cause energy shifts are incorporated here. These operators can be written as [24]

$$\begin{aligned}
H_1(\mathbf{r}) &= -\frac{\alpha^2}{2}\mathbf{p}^4, \\
H_{4'}(\mathbf{r}) &= \frac{\alpha^2}{2}\pi Z\delta(\mathbf{r}), \\
H_{4''}(\mathbf{r}_{12}) &= -\alpha^2\pi\delta(\mathbf{r}_{12}), \\
H_2(\mathbf{r}_{12}) &= -\frac{\alpha^2}{2}\frac{1}{r_{12}} \left[\mathbf{p}_1 \cdot \mathbf{p}_2 + \frac{\mathbf{r}_{12}(\mathbf{r}_{12} \cdot \mathbf{p}_1) \cdot \mathbf{p}_2}{r_{12}^2} \right], \\
H_{5''}(\mathbf{r}_{12}) &= -\frac{8}{3}\alpha^2\pi\mathbf{s}_1 \cdot \mathbf{s}_2\delta(\mathbf{r}_{12}).
\end{aligned} \tag{11}$$

The matrix elements for two one-particle operators H_1 and $H_{4'}$ are equal in zero approximation for all Q states, therefore

$$\langle Q|H_1+H_{4'}|Q\rangle^{(0)} = -\alpha^2Z^4\sum_i q(n_i l_i)E_0^R(n_i l_i), \tag{12}$$

where

$$E_0^R(nl) = -\frac{2}{n^3} \left[\frac{2}{2l+1} - \frac{3}{4n} - \delta(1,0) \right]. \tag{13}$$

In our case the numerical evaluation of Eq. (12) yields

$$\begin{aligned}
\langle Q|H_1+H_{4'}|Q\rangle^{(0)} &= -\alpha^2Z^4 \left[\frac{1}{8}k_1 + \frac{5}{128}k_2 + \frac{7}{384}k_3 + \frac{1}{72}k_4 + \frac{5}{648}k_5 + \frac{1}{360}k_6 \right. \\
&\quad + \frac{13}{2^{11}}k_7 + \frac{23}{3 \times 2^{11}}k_8 + \frac{17}{5 \times 2^{11}}k_9 \\
&\quad \left. + \frac{11}{7 \times 2^{11}}k_{10} + \frac{27}{5000}k_{11} + \frac{31}{15000}k_{12} \right]. \tag{14}
\end{aligned}$$

We further note that the zero-order approximation for the three-particle operators H_2 , $H_{5''}$, and $H_{4''}$ are proportional to Z^3 . Thus

$$\langle Q|H_2+H_{4''}+H_{5''}|Q\rangle^{(0)} \cong \alpha^2Z^3F(Q). \tag{15}$$

The calculation of $F(Q)$ is described in detail in [24]. It is sufficient to calculate only the two radial integrals, T and K ,

$$T(n_1 l_1 n_2 l_2; n_4 l_4 n_3 l_3) = \int_0^\infty r_1^2 dr R_{n_1 l_1}(r_1) R_{n_2 l_2}(r_2) R_{n_4 l_4}(r_2) R_{n_3 l_3}(r_1), \quad (16)$$

$$K_l(n_1 l_1 n_2 l_2; n_4 l_4 n_3 l_3) = \int_0^\infty r_1^2 dr_1 \int_0^\infty r_2^2 dr_2 \theta(r_1 - r_2) \frac{r_2^l}{r_1^{l+1}} R_{n_1 l_1}(r_1) R_{n_2 l_2}(r_2) \frac{d^2}{dr_1 dr_2} R_{n_4 l_4}(r_2) R_{n_3 l_3}(r_1). \quad (17)$$

Moreover, the angular part for the two-particle operators $H_2 + H_{4''} + H_{5''}$ is the same as for the $1/r_{12}$ electrostatic operator. Hence, Eqs. (2)–(5) can be applied to evaluate the corresponding relativistic matrix elements. The same equations have also been used to determine the first-order corrections originating from the one-particle operators H_1 and $H_{4'}$. The radial part of the relativistic first-order contribution is [24]

$$E_k^i(n_1 l_1 n_2 l_2; n_4 l_4 n_3 l_3) = \sum_n \frac{1}{E_n + E_{n_2} - E_{n_4} - E_{n_3}} \begin{bmatrix} l & l_1 & l_3 \\ 0 & 0 & 0 \end{bmatrix} \begin{bmatrix} l & l_2 & l_4 \\ 0 & 0 & 0 \end{bmatrix} M^i(nl, n_1 l_1) R_k(n_1 l_1 n_2 l_2; n_4 l_4 n_3 l_3), \quad (18)$$

with

$$M^i(nl, n'l') = -\frac{1}{2} \delta(l, l') \int_0^\infty r^2 dr \left[\frac{2}{r} - \frac{1}{n^2} \right] \left[\frac{2}{r} - \frac{1}{(n')^2} \right] R_{nl}(r) R_{n'l'}(r), \quad (19)$$

$$M^{4'}(nl, n'l') = -\frac{1}{2} \delta(l, 0) \delta(l', 0) R_{nl}(0) R_{n'l'}(0). \quad (20)$$

Summation in (15) extends over the discrete part of the spectrum and includes integration over the continuous part [24]. In this study we have calculated all the relevant expressions, i.e., T , K_1 , E_k^1 , and $E_k^{4'}$ for all possible nl values associated with different Q states. In particular, we have found that all terms scale as Z^3 and hence

$$\langle Q | H_2 + H_{4''} + H_{5''} | Q \rangle^{(0)} + \langle Q | H_1 + H_{4'} | Q \rangle^{(1)} = \alpha^2 Z^3 E_1^R(Q). \quad (21)$$

Here we have evaluated $E_1^R(Q)$ for the inner $1s$, $2s$, $2p$, $3s$, $3p$, and $3d$ shells

$$\begin{aligned} E_1^R(1s^k 1s^k 2s^k 2p^k 3s^k 3s^k 3p^k 3s^k 3d^k 3d^k) \\ = \frac{k_1}{2}(k_1 - 1)0.480140 + \frac{k_2}{2}(k_2 - 1)0.0608865 + \frac{k_3}{2}(k_3 - 1)0.0440925 + \frac{k_4}{2}(k_4 - 1)0.0190056 \\ + \frac{k_5}{2}(k_5 - 1)0.0128910 + \frac{k_6}{2}(k_6 - 1)0.00757975 + \frac{k_7}{2}(k_7 - 1)0.00802 + \frac{k_8}{2}(k_8 - 1)0.00544 \\ + \frac{k_9}{2}(k_9 - 1)0.00320 + \frac{k_{10}}{2}(k_{10} - 1)0.00250 + \frac{k_{11}}{2}(k_{11} - 1)0.00411 + \frac{k_{12}}{2}(k_{12} - 1)0.00278 \\ + k_1 k_2 0.100071 + k_1 k_3 0.0817048 + k_1 k_4 0.039433 + k_1 k_5 0.0321032 + k_1 k_6 0.011363 \\ + k_1 k_7 0.018886 + k_1 k_8 0.015372 + k_1 k_9 0.006766 + k_1 k_{10} 0.003073 + k_1 k_{11} 0.010278 \\ + k_1 k_{12} 0.008345 + k_2 k_3 0.049104 + k_2 k_4 0.0250261 + k_2 k_5 0.022652 + k_2 k_6 0.015815 \\ + k_2 k_7 0.03355 + k_2 k_8 0.011327 + k_2 k_9 0.007649 + k_2 k_{10} 0.003737 + k_2 k_{11} 0.007570 \\ + k_2 k_{12} 0.006378 + k_3 k_4 0.025932 + k_3 k_5 0.019465 + k_3 k_6 0.012703 + k_3 k_7 0.013422 \\ + k_3 k_8 0.010158 + k_3 k_9 0.006786 + k_3 k_{10} 0.003270 + k_3 k_{11} 0.007608 + k_3 k_{12} 0.005763 \\ + k_4 k_5 0.01286 + k_4 k_6 0.00531 + k_4 k_7 0.01331 + k_4 k_8 0.00823 + k_4 k_9 0.00391 \\ + k_1 k_{10} 0.003737 + k_4 k_{11} 0.007570 + k_4 k_{12} 0.00493 + k_5 k_6 0.00552 + k_5 k_7 0.01367 \\ + k_5 k_8 0.00834 + k_5 k_9 0.00400 + k_5 k_{10} 0.00203 + k_5 k_{11} 0.00797 + k_5 k_{12} 0.00498 \\ + k_6 k_7 0.01424 + k_6 k_8 0.00873 + k_6 k_9 0.00418 + k_6 k_{10} 0.00216 + k_6 k_{11} 0.00819 \\ + k_6 k_{12} 0.00514 + k_7 k_8 0.00537 + k_7 k_9 0.00302 + k_7 k_{10} 0.00151 + k_7 k_{11} 0.00680 \\ + k_7 k_{12} 0.00433 + k_8 k_9 0.00306 + k_8 k_{10} 0.00153 + k_8 k_{11} 0.00704 + k_8 k_{12} 0.00436 \\ + k_9 k_{10} 0.00162 + k_9 k_{11} 0.00725 + k_9 k_{12} 0.00451 + k_{10} k_{11} 0.00750 + k_{10} k_{12} 0.00467 + k_{11} k_{12} 0.00456. \quad (22) \end{aligned}$$

TABLE I. Range of $3d$ - $2p$ transitions for Xe ions with $2p$ vacancies.

| Number of $2p$ holes | X-ray energies (eV) | Approximate width of structure (eV) | Energy shift (eV) | Radiative transition probabilities (10^{13} s^{-1}) |
|----------------------|---------------------|-------------------------------------|-------------------|---|
| 1 | 4053–4647 | 594 | 102 | 5.4–51.0 |
| 2 | 4147–4749 | 602 | 102 | 11.7–109.0 |
| 3 | 4243–4851 | 608 | 102 | 18.7–137.9 |
| 4 | 4339–4955 | 616 | 104 | 26.6–248.6 |
| 5 | 4437–5060 | 623 | 105 | 35.4–331.3 |
| 6 | 4536–5166 | 630 | 106 | 45.2–423.7 |

The zero- (E_0^R) and first- (E_1^R) order energies can be represented in the form of a screening formula similar to Eq. (8) for $E^N(Q)$,

$$E^R(Q) = \alpha^2 Z E_0^R(Q) \left[Z + \frac{E_1^R(Q)}{3E_0^R(Q)} \right]^3. \quad (23)$$

Then the resulting total energy $E(Q)$ can be expressed as

$$E(Q) = E^N(Q) + E^R(Q), \quad (24)$$

where $E^N(Q)$ and $E^R(Q)$ are the nonrelativistic and relativistic contributions, respectively. Finally the x-ray transition energies may be written as

$$\begin{aligned} E(Q) - E([n_1 l_1]^{-1} n_2 l_2 Q) \\ = [E^N(n_1 l_1) - E_0^N(n_2 l_2)] (Z - \sigma^N)^2 \\ + \alpha^2 Z [E_0^R(n_1 l_1) - E_0^R(n_2 l_2)] (Z - \sigma^R)^3, \end{aligned} \quad (25)$$

where σ^N and σ^R are equal to

$$\begin{aligned} \sigma^N &= - \frac{\{E_1^N(Q) - E_1^N([n_1 l_1]^{-1} n_2 l_2 Q)\}}{2[E_0^N(n_1 l_1) - E_0^N(n_2 l_2)]}, \\ \sigma^R &= - \frac{\{E_1^R(Q) - E_1^R([n_1 l_1]^{-1} n_2 l_2 Q)\}}{3[E_0^R(n_1 l_1) - E_0^R(n_2 l_2)]}. \end{aligned} \quad (26)$$

As a representative example the relevant $2p$ - $3d$ x-ray energies (Q - $2p^{-1}3dQ$) are discussed in more detail.

For each L spectrum correlated with a specific $2p$ -hole state, i.e.,

$$\begin{aligned} \Phi_0 \Phi_1 - 2p^{-1} 3d \Phi_0 \Phi_1, \\ \Phi_0 = 1s^2 2s^2 2p^6, \\ \Phi_1 = 3s^{k_4} 3p^{k_5} 3d^{k_6} 4s^{k_7} 4p^{k_8} 4d^{k_9} 5s^{k_{11}} 5p^{k_{12}}. \end{aligned} \quad (27)$$

$$W(Q, [n_1 l_1]^{-1} n_2 l_2 Q) = A_0(n_1 l_1, n_2 l_2) Z^4 \frac{k_1}{g_1} \left[1 - \frac{k_2}{g_2} \right] \left[\frac{E(Q) - E([n_1 l_1]^{-1} n_2 l_2 Q)}{E_0(Q) - E_0([n_1 l_1]^{-1} n_2 l_2 Q)} \right]^3 \left[1 - \frac{P(k_1)}{Z} \right]^2, \quad (28)$$

where $g_i = 2(2l_i + 1)$ are the statistical weights and $P(k_i)$ the first-order correction for dipole matrix elements. The hydrogenic transition probabilities A_0 (10^8 s^{-1}) are listed in Table III. It is evident from this table that the $3d$ - $2p$, $4d$ - $2p$, $4f$ - $3d$, and $5g$ - $4f$ transitions are characterized by large transition probabilities. For the L spectra we expect the $2p$ - $3d$ decays to dominate the observed x-ray

350 different $2p$ - $3d$ transition energies have been calculated [17,23]. Due to the limited resolution of our x-ray detector, these lines have been treated as a quasicontinuum with an energy-band width of roughly 600 eV. $2p$ - $3d$ transitions with ten electrons have the largest energy values while those transitions with the maximum number of electrons ($N \leq 53$) are shifted to lower energies by about 600 eV. The energy range of $3d$ - $2p$ transitions for different $2p$ hole configurations in Xe are summarized in Table I.

The key parameters in our theoretical model of multiply core-excited states are the occupation numbers k_i , in particular, the number of $2p$ and $3d$ electrons are of primary importance. Table I clearly indicates that changing the number of $2p$ vacancies by one shifts the L x-ray energies by about 102–106 eV. On the other hand, adding one extra $3d$ electron decreases the energy by about 26 eV. To obtain accurate L and M x-ray energies, relativistic corrections have been included in the calculation. As an illustrative example we present here relativistic corrections for $3d$ - $2p$ transitions characterized by $1s^2 2s^2 2p^k - 1s^2 2s^2 2p^{k-1}$ with varying initial $2p^k$ hole states, where k is ranging from $k=1$ to 6. As can be seen relativistic corrections for the $3d$ - $2p$ decay are of the order 119–141 eV, depending on the specific $2p^k$ core states (see Table II). These results agree within a few eV with recent multiconfiguration Dirac-Fock calculations.

C. Transition probabilities

In this study we have also investigated transition probabilities within the framework of the LS -averaged approximation. As an example we present here the analytic formula for LS -averaged transition probabilities

TABLE II. Relativistic corrections for $3d$ - $2p$ transitions characterized by $1s^2 2s^2 2p^k - 1s^2 2s^2 2p^{k-1} 3d$ initial-to-final-state configurations.

| k | 1 | 2 | 3 | 4 | 5 | 6 |
|------------|-----|-----|-----|-----|-----|-----|
| E^R (eV) | 149 | 141 | 135 | 130 | 124 | 119 |

TABLE III. Averaged hydrogenic transition probabilities $A_0(nl, n'l')$ in units of 10^8 s^{-1} .

| $nl-n'l'$ | A_0 | $nl-n'l'$ | A_0 | $nl-n'l'$ | A_0 | $nl-n'l'$ | A_0 |
|-----------|----------|-----------|-----------|-----------|----------|-----------|----------|
| $2p-1s$ | 37.575 | $3s-2p$ | 0.1262 | $3d-2p$ | 6.4625 | $4p-3d$ | 0.020 84 |
| $3p-1s$ | 10.106 | $4s-2p$ | 0.051 54 | $4d-2p$ | 2.0617 | $5p-3d$ | 0.008 97 |
| $4p-1s$ | 4.0896 | $5s-2p$ | 0.025 76 | $5d-2p$ | 0.9422 | $6p-3d$ | 0.004 69 |
| $5p-1s$ | 2.0617 | $6s-2p$ | 0.014 02 | $6d-2p$ | 0.4906 | $5p-4d$ | 0.011 30 |
| $6p-1s$ | 1.1706 | $4s-3p$ | 0.036 69 | $4d-3p$ | 0.7035 | $6p-4d$ | 0.005 65 |
| $3p-2s$ | 1.3464 | $5s-3p$ | 0.018 09 | $5d-3p$ | 0.3390 | $4f-3d$ | 1.9296 |
| $4p-2s$ | 0.5799 | $6s-3p$ | 0.010 14 | $6d-3p$ | 0.1877 | $5f-3d$ | 0.6356 |
| $5p-2s$ | 0.2968 | $5s-4p$ | 0.012 90 | $5d-4p$ | 0.1485 | $6f-3d$ | 0.3003 |
| $6p-2s$ | 0.1635 | $6s-4p$ | 0.007 162 | $6d-4p$ | 0.086 18 | $5f-4d$ | 0.3617 |
| $4p-3s$ | 0.1838 | | | $5d-4f$ | 0.050 46 | $6f-4d$ | 0.1801 |
| $5p-3s$ | 0.077 70 | | | $6d-4f$ | 0.021 44 | $5g-4f$ | 0.7654 |
| $6p-3s$ | 0.057 28 | | | | | $6g-4f$ | 0.2470 |
| $5p-4s$ | 0.044 21 | | | | | | |
| $6p-4s$ | 0.026 73 | | | | | | |

features. Furthermore, from Table III it may be inferred that $3d-4f$ transitions are of major significance for the observed *M* x-ray spectra. The experimental results are discussed in the following section.

IV. RESULTS AND DISCUSSION

Figure 1 gives an overview of the observed x-ray spectra originating from Xe⁴⁴⁺ to Xe⁴⁸⁺ ions impinging on Cu surfaces. As can be seen the Xe⁴⁴⁺ spectrum [Fig. 1(a)] consists only of lower-energy *M* x-ray peaks due to the missing *L* vacancy states of the incoming projectile ion. From this figure we can also deduce that no additional *L*-shell vacancies are produced during the impact of the ion on the surface. In contrast the spectra resulting from Xe⁴⁵⁺ to Xe⁴⁸⁺ initial projectiles show, as expected, higher-energy *L* x-ray-line structures, which arise

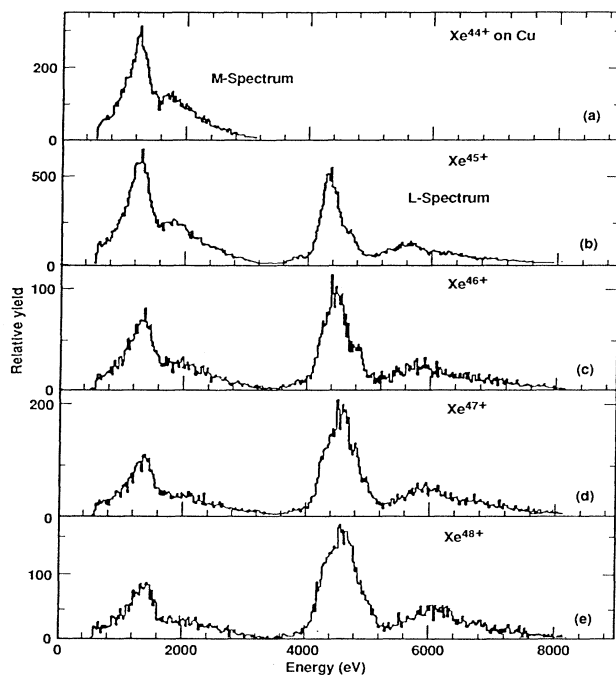


FIG. 1. (a)–(e) Xe *M, L* x-ray spectra following $7q$ keV Xe^{*q*} ($q = 44-48$) ion impact on a Cu surface as a function of the projectile charge q .

predominantly from electric-dipole transitions into empty $2p$ states. In accordance with the increasing number of $2p$ vacancies (see Table I and the Appendix), the measured *L* line energy positions shift towards higher energies with increased charge state q . Due to many satellite-line groups and limited energy resolution of our Si (Li) detector the observed line intensities are averaged over several closely spaced line groups. For the following discussion we have displayed the Xe⁴⁴⁺, Xe⁴⁵⁺, and Xe⁴⁸⁺ spectra in more detail in Figs. 2(a)–2(c). For a comparison we have indicated the range of the calculated $2p-3d$ transition energies in Figs. 2(b) and 2(c) for the satellite groups originating from $1s^2 2s^2 2p^k$ ($k = 2-5$) initial inner-hole-state configurations. These include about 350 possible satellite groups (see the Appendix) with centroid energies varying from 4053 to 5166 eV for Xe⁴⁵⁺ and 4×350 satellite groups for Xe⁴⁸⁺ projectiles with a total-energy variation of about 4053 to 4955 eV. The simplest case is Xe⁴⁵⁺, where the projectile ion arrives at the surface with only one $2p$ hole. The following configurations of multiply excited states with main quantum numbers $n \leq 4$ and angular-momentum states $l \leq 2$ were con-

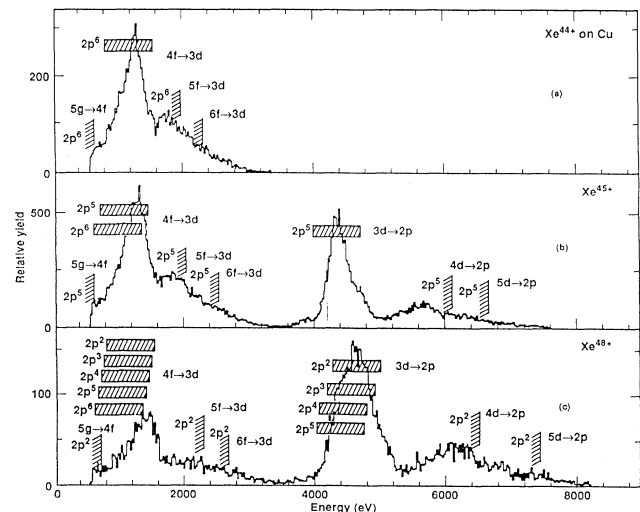


FIG. 2. Comparison of observed and predicted x-ray structures for (a) Xe⁴⁴⁺, (b) Xe⁴⁵⁺, and (c) Xe⁴⁸⁺.

line intensities and the group of L lines shift to higher energies with increasing number of L vacancies. A comparison of the experimental data with calculated transition energies and rates originating from $n=3-5$ states suggests that transitions of the type $3d-2p$ dominate for the L spectra and $4f-3d$ for the M line structures, where $4f$ states cannot directly decay to the $2p$ states. In addition, we have also observed weaker transitions arising from $4d-2p$ and $5d-2p$ as well as $5g-4f$.

The discussion of charge-transfer processes and time scales involved when highly charged Xe ions impinge on a Cu surface suggest the following picture: During the approach on the way in to the surface highly excited states ($n \cong 20-40$) are formed. These so-called "hollow atoms" survive until the ions hit the surface. Those ions penetrating into the solid interact with single Cu atoms, leading to a side feeding of $n \geq 3$ states, which give rise to the observed x-ray lines, energies, and intensity ratios.

ACKNOWLEDGMENTS

This work was performed in part under the auspices of the U.S. Department of Energy by Lawrence Livermore National Laboratory under Contract No. W-7405-Eng-48. One of us (R.B.) would like to thank the members of the Institute of Spectroscopy, Russian Academy of Sciences, Troitsk and the Manne Siegbahn Institute of Physics, Stockholm for their hospitality and financial support. We are also indebted to F. Hao and T. Tanaka from the University of Nevada, Reno for stimulating discussions.

APPENDIX

As a representative example the relevant $2p-3d$ x-ray energies ($Q-2p^{-1}3dQ$) are given in Tables IV-IX with

respect to the number of initial $2p$ vacancies. Thus Table IV shows the energy values in eV for radiative transitions of the type

$$\begin{aligned} & \Phi_0 \Phi_1 - 2p^{-1} 3d \Phi_0 \Phi_1, \\ & \Phi_0 = 1s^2 2s^2 2p^6, \\ & \Phi_1 = 3s^k 3p^k 3d^k 4s^k 4p^k 4d^k 5s^k 5p^k. \end{aligned} \quad (\text{A1})$$

This table is divided into I-XI columns, depending on the initial number of electrons in the system. As can be seen in the first column labeled I, the $3d$ subshell becomes progressively filled ($\Phi_1 = 3d^k$). The next column (II) gives the corresponding energy values for Φ_1 with different numbers of electrons in all subshells except $3d$, by occupying first $3s^k$, then $3p^k$, and so on. Initially, all outer subshells are filled. The columns labeled III-XI are organized in an analogous way, but by progressively adding one $3d$ electron for every new column. The key parameters in our theoretical mode of multiply core-excited states are the occupation numbers k_i ; in particular, the number of $2p$ and $3d$ electrons are of primary importance. The data listed in Tables IV-IX clearly indicate that changing the number of $2p$ vacancies by one sifts the L x-ray energies above 100 eV. On the other hand, adding one extra $3d$ electron decreases the energy by about 20-30 eV.

For each L spectrum correlated with a specific $2p$ -hole state, i.e.,

$$\Phi_0 = 1s^2 2s^2 2p^k \quad (k=6 \text{ to } 1),$$

350 different $2p-3d$ transition energies have been calculated.

*Present address: Department of Physics, University of Nevada, Reno, Reno, NV 89557.

- [1] H. J. Andr a, in *Atomic Physics of Highly Charged Ions*, edited by R. Marrus (Plenum, New York, 1989).
- [2] D. H. Schneider, M. Clark, B. M. Penetrante, J. McDonald, D. DeWitt, and J. N. Bardsley, *Phys. Rev. A* **44**, 3119 (1991).
- [3] J. P. Briand, L. de Billy, P. Charles, Essabaa, P. Briand, R. Geller, J. P. Desclaux, S. Bliman, and C. Ristori, *Phys. Rev. Lett.* **65**, 159 (1990).
- [4] E. D. Donets, *Phys. Scr.* **T3**, 11 (1983).
- [5] M. Delaunay, S. Dousson, R. Geller, B. Jaquot, D. Hitz, P. Ludwig, P. Sortais, and S. Bliman, *Nucl. Instrum. Methods B* **23**, 177 (1987).
- [6] M. St ockli, C. L. Cocke, and P. Richard, *Rev. Sci. Instrum.* **61**, 242 (1990).
- [7] F. W. Meyer, *J. Phys. (Paris)* **50**, C1-263 (1989).
- [8] S. T. de Zwart, *Nucl. Instrum. Methods B* **23**, 239 (1987).
- [9] L. Folkerts and R. Morgenstern, in *Atomic Physics of Highly Charged Ions*, edited by E. Salzborn, P. H. M okler, and A. M uller (Springer, Berlin, 1991); *Z. Phys. D* **21**, S351 (1991).
- [10] H. J. Andr a, A. Simionovici, T. Lamy, A. Brenac, G. Lambole, S. Andriamonje, J. J. Bonnet, A. Fleury, M. Bonnefoy, M. Chassevent, and A. Pesnelle, in *Atomic Physics of Highly Charged Ions*, edited by E. Salzborn, P. H. M okler, A. M uller (Springer, Berlin, 1991); *Z. Phys. D* **21**, S135 (1991).
- [11] E. D. Donets, *Nucl. Instrum. Methods B* **9**, 522 (1985).
- [12] D. Schneider, D. DeWitt, M. W. Clark, R. Schuch, C. L. Cocke, R. Schmieder, K. J. Reed, M. H. Chen, R. E. Marrs, M. Levine, and R. Fortner, *Phys. Rev. A* **42**, 3889 (1990).
- [13] C. P. Bhalla, *Phys. Rev. A* **8**, 2877 (1973); private communication.
- [14] E. D. Donets, S. V. Kartashose, and V. P. Ovsyannikov (unpublished).
- [15] Y. Conturie, B. Yaakobi, U. Feldman, G. A. Doschek, and R. D. Cowan, *J. Opt. Soc. Am.* **71**, 1309 (1981).
- [16] P. A. Zeijlmans van Emmichoven, C. C. Havener, and F. W. Meyer, *Phys. Rev. A* **43**, 1405 (1991).
- [17] U. I. Safronova, R. Bruch, and D. Schneider, *Phys. Scr.* (to be published).
- [18] S. Salomonson and P. Oster, *Phys. Rev. A* **41**, 4670 (1990).
- [19] S. Salomonson and P. Oster, *Phys. Rev. A* **40**, 5548 (1989).
- [20] E. Lindroth and S. Salomonson, *Phys. Rev. A* **41**, 4659

- (1990).
- [21] C. Froese Fischer, *The Hartree-Fock Method for Atoms* (Wiley, New York, 1977).
- [22] R. D. Cowan, *The Theory of Atomic Structure and Spectra* (University of California, Berkeley, 1981), and references given therein.
- [23] U. I. Safranova, I. Yu. Tolstikhina, R. Bruch, T. Tanaka, F. Hao, and D. Schneider, Phys. Scr. (to be published).
- [24] E. V. Aglitskii and U. I. Safranova, *Spectroscopy of Autoionizing States of Atomic Systems* (Energoatomizdat, 1985).
- [25] I. A. Ivanov and U. I. Safranova, Opt. Spektrosk. **65**, 5 (1985) [Opt. Spectrosc. **65**, 2 (1988)].
- [26] A. V. Vinogradov and U. I. Safranova, Opt. Spektrosk. **52**, 787 (1982) [Opt. Spectrosc. **52**, 471 (1982)].
- [27] L. A. Vainshtein, A. V. Vinogradov, I. R. Rublev, and U. I. Safranova, Opt. Spektrosk. **48**, 424 (1980) [Opt. Spectrosc. **48**, 234 (1980)].
- [28] U. I. Safranova and V. S. Senashenko, J. Phys. B **14**, 603 (1981).
- [29] P. A. Burke and W. Eissner, in *Atoms in Astrophysics*, edited by P. A. Burke, W. B. Eissner, D. A. Hummer, and I. C. Percival (Plenum, New York, 1983), p. 17.
- [30] G. Omar and Y. Hahn, Phys. Rev. A **43**, 4695 (1991).
- [31] J. Burgdörfer, P. Lerner, and F. Meyer, Phys. Rev. A **44**, 5674 (1991).